Mechanical, electrical, thermal and tribological behavior of epoxy resin composites reinforced with waste hemp-derived carbon fibers

J Mater Sci

Composites & nanocomposites

Mechanical, electrical, thermal and tribological behavior of epoxy resin composites reinforced with waste hemp-derived carbon fibers

Mattia Bartoli[1,2], Donatella Duraccio[3,*], Maria Giulia Faga[3], Erik Piatti[4], Daniele Torsello[4,5], Gianluca Ghigo[4,5], and Giulio Malucelli[2,6]

[1] *Center for Sustainable Future Technologies, Italian Institute of Technology, Via Livorno 60, 10144 Torino, Italy*
[2] *Consorzio Interuniversitario Nazionale per la Scienza e Tecnologia dei Materiali (INSTM), Via G. Giusti 9, 50121 Firenze, Italy*
[3] *Institute of Sciences and Technologies for Sustainable Energy and Mobility, National Council of Research, Strada delle Cacce 73, 10135 Torino, Italy*
[4] *Department of Applied Science and Technology, Politecnico di Torino, C.so Duca degli Abruzzi 24, 10129 Torino, Italy*
[5] *Istituto Nazionale di Fisica Nucleare, Sez. Torino, Via P. Giuria 1, 10125 Torino, Italy*
[6] *Department of Applied Science and Technology, Politecnico di Torino, Viale Teresa Michel 5, 15121 Alessandria, Italy*

Received: 25 March 2022
Accepted: 15 July 2022

ABSTRACT

Short hemp fibers, an agricultural waste, were used for producing biochar by pyrolysis at 1000 °C. The so-obtained hemp-derived carbon fibers (HFB) were used as filler for improving the properties of an epoxy resin using a simple casting and curing process. The addition of HFB in the epoxy matrix increases the storage modulus while damping factor is lowered. Also, the incorporation of HFB induces a remarkable increment of electrical conductivity reaching up to 6 mS/m with 10 wt% of loading. A similar trend is also observed during high-frequency measurements. Furthermore, for the first time wear of these composites has been studied. The use of HFB is an efficient method for reducing the wear rate resistance and the friction coefficient (COF) of the epoxy resin. Excellent results are obtained for the composite containing 2.5 wt% of HFB, for which COF and wear rate decrease by 21% and 80%, respectively, as compared with those of the unfilled epoxy resin. The overall results prove how a common waste carbon source can significantly wide epoxy resin applications by a proper modulation of its electrical and wear properties.

Handling Editor: Gregory Rutledge.

Address correspondence to E-mail: donatella.duraccio@stems.cnr.it

https://doi.org/10.1007/s10853-022-07550-9

Published online: 02 August 2022

GRAPHICAL ABSTRACT

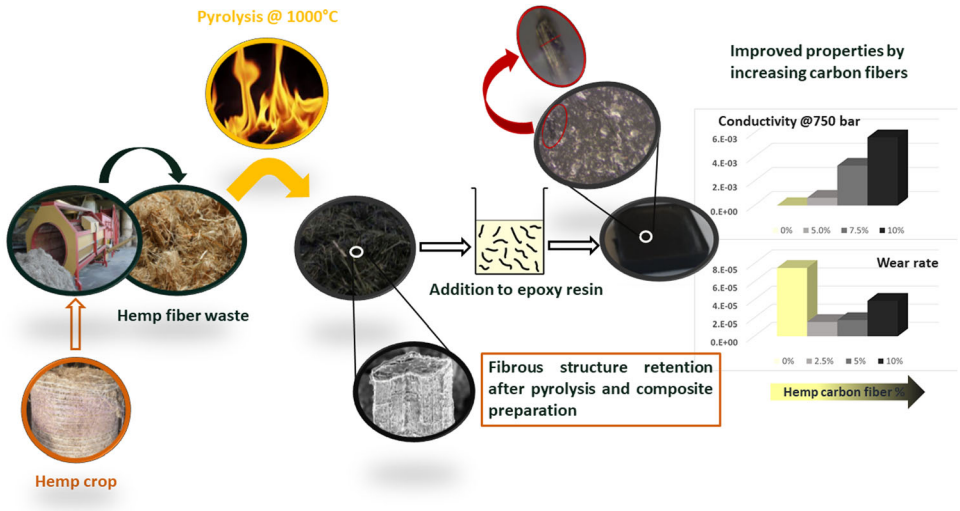

Introduction

In industry, epoxy resins are one of the most common and widely used thermosets. This is because of their high stiffness, high tensile strength and excellent chemical resistance [1]. Epoxy resins find different interesting uses: they are employed in the aerospace sector as laminates due to their very high strength-to-weight ratio when compared with steel and aluminum alloys [2]; in the automotive sector, they act as adhesives replacing welding and as structural components [3]. In the electronic industry, circuit boards, diodes, capacitors and transistors are manufactured with epoxy resins [4]. However, they exhibit low electrical conductivity [5] and inadequate tribological properties [6]. In order to overcome these issues, different fillers have been dispersed into epoxy systems. Among them, bioderived fillers have risen attention due to the diffusion of environment preservation policies that have boosted the cultivation of crops able to act as platforms for multiple products manufacture [7]. Hemp crops are one of the most outstanding case in the field [8] and are able to provide valuable sources for plenty of applications ranging from textile to other relevant industrial sectors [9]. Among all hemp-derived products, hemp fibers are the most inexpensive, readily available and most employed for the production of reinforced materials in cementitious and polymer matrices [10]. As reported by Scarponi et al. [11], epoxy-hemp fiber composites reach comparable performances with E-glass fiber-based materials, but with a considerably reduced environmental footprint. However, hemp fiber-reinforced composites show very high water absorption [12] that significantly reduces the durability of the material [13]. Also, it is reported that epoxy–carbon fibers composites have superior mechanical performance with respect to epoxy–hemp counterparts [14] and that carbon fibers show a remarkable electrical and thermal conductivity [15] while hemp fiber-containing composites are natural insulators [16–18]. For all these reasons, in this work, short damage hemp fibers not suitable for other applications have been converted into carbonaceous ones through pyrolysis [19]. The so-obtained biochar, with the original fiber shape retained, has been used for the first time as filler in an epoxy resin. It is well known that the impact of carbonaceous materials produced from pyrolysis (known as biochars) in different applications has been growing in recent years[20, 21]. Furthermore, despite biochar high production temperatures [22] and high filler loading [23] necessary for affecting the bulk properties of the matrix (usually beyond 20 wt%) [24]), it has been

proved to be a valuable choice for the production of conductive epoxy composites [25] with performances comparable to those achieved by the incorporation of carbon nanotubes [26]. The clear advantage of the biochar as compared to the petroleum-based carbon filler for composites fabrication is its waste utilization and re-use resources which aids the circular economy, sustainability and reduction of environmental footprint [27]. Interestingly, hemp fiber biochar (HFB) could represent a good solution to produce conductive composites with low percolation threshold due to its high aspect ratio. It is also expected that HFB can improve the tribological performance of epoxy resin as found for some other carbonaceous filler [6]. Katiyar et al. [6], for example, have found that graphene and graphite inclusion at 5 wt% in the epoxy matrix decreases its friction coefficient, though with high wear track width. Cui et al. [28] have found that acid-MWCNT and amino-MWCNT, prepared by carboxylation and amidation method, are able to improve the tribological behavior of epoxy networks.

In this light, we have thoroughly studied the dynamic-mechanical, tribological and electrical (DC and AC) properties of epoxy-HFB composites containing different amounts of fibers (ranging from 2.5 to 10 wt%). Hardness measurements, thermal and thermogravimetric analyses complete the characterization, providing a comprehensive overview of the influence of HFB on the epoxy resin.

Materials and methods

Materials

Waste short hemp fibers (length below 10 cm) were kindly supplied by Assocanapa s.r.l. They were obtained by field-retted hemp stalks using a prototype machine patented by Assocanapa and CNR [29], able to separate shives from fibers. Short damage fibers not suitable for other applications were collected and used without further treatment. Hemp fibers were pyrolyzed in a tubular furnace (Carbolite TZF 12/65/550) in nitrogen atmosphere, with a heating rate of 15 °C/min, reaching a final temperature of 1000 °C. The system was kept at 1000 °C for 30 min and cooled down at room temperature in nitrogen atmosphere.

Diglycidyl ether of bisphenol-A epoxy resin (average M_n: ~ 377; density: 1.16 g/mL at 25 °C) and diethylene triamine (curing agent) were purchased from Sigma-Aldrich (Milano, Italy). The resin and hardener were thoroughly mixed in a ratio of 2 parts to 3 parts, respectively. The fibers were dispersed into the epoxy monomer using a tip ultrasonicator apparatus (Sonics Vibra-cell) for 15 min, operating at room temperature. Finally, the mixture was poured in a silicon mold of different shapes according to the subsequent analytical technique. The unfilled epoxy polymer was coded as EP. The weight fractions of EP/HFB were 97.5/2.5, 95/5, 92.5/7.5, 90/10. The composites were left to cure for 6 h at room temperature before being removed from the mold. Post-curing was continued for two hours in a ventilated oven at 80 °C.

Methods

The morphology of HFB was investigated using field emission scanning electrical microscopy (FESEM, Zeis SupraTM 40, Oberkochen, Germany), whereas the distribution of HFB in the epoxy matrix was evaluated through optical microscopy (Carl Zeiss Axiolab A1 m, Oberkochen, Germany).

The electric transport measurements on biochar derived from hemp fibers were performed in the four-wire configuration by electrically contacting the biochar samples with thin gold wires and conducting silver paste. A constant current, I = 100 mA, was applied between the outer current contacts with a B2912 source-measure unit, and the longitudinal voltage drop that occurred across the inner voltage contacts, V_{xx}, was measured with a 34,420 nanovoltmeter (Keysight Technologies, Santa Rosa, CA, USA). Thermoelectric voltages were removed by inverting the sourced current within each resistance measurement. The temperature dependence of the electric resistance, $R = V_{xx}/I$, was measured by loading the samples in the high-vacuum chamber of an ST-403 pulse-tube cryocooler (Cryomech, Syracuse, NY, USA), cooling the system to the base temperature of 2.7 K, and then allowing the samples to quasi-statically heat up to 300 K due to the residual thermal coupling to the outside environment. Then, the sheet resistance was calculated as $R_s = R \cdot w/l$, where w and l are the length and width of the sample between the voltage contacts, respectively, and the sheet conductance as $G_s = 1/R_s$.

Neat and pyrolyzed hemp fibers were analyzed through FTIR (Nicolet 5700, Thermoscientific,

Waltham, USA) in attenuated total reflectance (ATR) mode (Smartorbit, Thermoscientific) in the range from 500 to 4000 cm^{-1} with a resolution of 2 cm^{-1}.

HFB was analyzed by Raman spectroscopy in the range from 500 to 3500 cm^{-1}: To this aim, a Renishaw® Ramanscope InVia (H43662 model, Gloucestershire, UK) equipped with a green laser light source at 514 nm was employed.

Weight loss measurements were performed using a Pyris1 TGA apparatus (Perkin Elmer, USA). The temperature was reproducible to 1 °C and the mass to 0.5%. A specimen size of approximately 15 mg cut into small pieces, facilitating heat transfer and the escape of the volatile products, was used [30]. The samples were heated from 50 to 700 °C at 10 °C/min under both N_2 gas and air flow (40 mL/min).

The thermal behavior of the composite was assessed by using a Mettler DSC-822 apparatus. DSC analyses were carried out by heating about 8 mg of sample from 25 °C to 160 °C at a rate of 10 °C/min; the glass transition temperature (T_g) was taken by applying the first derivative method. Calibration was performed using indium as standard (T_m = 156.4 °C; ΔH_m = 28.15 J/g).

DMTA tests (DMA Q800—TA Instruments) were carried out to study the thermomechanical properties of the epoxy composites under dynamic loading conditions and to determine the glass transition temperatures. The dual cantilever mode was used with fixed oscillation amplitude in strain-controlled mode (0.05%) and at 1 Hz. The temperature range varied from room temperature to 185 °C, applying a heating step of 3 °C/min. All the DMTA specimens were rectangular bars (size: 3 mm·6 mm·35 mm).

Shore D hardness was determined according to ASTM D2240 standard. Ten measurements were performed for each sample by using a Classic Durometer (model Sauter), and Spearman coefficient was calculated for evaluating the data correlation [31].

The surface roughness was measured with a Form Talysurf 120 contact profilometer. The R_a parameter, i.e., the arithmetic mean deviation of the surface profile, was obtained with a diamond conical stylus of 2 μm. The measurements were repeated ten times acquiring profile in different parts of the samples. Duncan's multiple range test was used for the statistical analysis ($p < 0.05$).

A CSEM High-Temperature Tribometer in ball-on-disk configuration was used for friction and wear measurements. A steel ball (100Cr6) of 6 mm in diameter ($R_a \sim 0.05$ mm) was used as the counter-body material. The sample, fixed on a support able to rotate, was 4 mm thick and with a square surface of 4 cm^2. For simulating severe conditions, tests were performed under 7 N load, 5 mm radius, and for a duration of 30.000 cycles without any lubricant. The average value of the friction coefficient at the steady state is the mean friction coefficient (COF), whose standard deviation was considered as a friction stability parameter [32].

Worn surfaces, at the end of the measurements, were gold-metalized with a layer of about 5 nm and observed by SEM (ZEISS EVO 50 XVP with LaB_6 source, equipped with detectors for secondary and backscattered electrons collection and EDS probe for elemental analyses). The wear depth and volume loss were measured by the contact profilometer described for roughness measurements. From the obtained 3D profiles, 2D profiles were extracted from different locations and the wear volume was calculated by integrating the surface area of the tracks over circumference length. The specific wear rate (k) was obtained by normalizing wear volume V (mm^3) to the applied load L (N) and to total sliding distance S (m) as shown in Eq. 1:

$$k = \frac{V}{SL} \tag{1}$$

The electrical resistance of composites was measured under increasing loads (up to 1500 bar) applied by an hydraulic press (Specac Atlas Manual Hydraulic Press 15 T, Orpington, UK) according to Giorcelli et al. [24]. Electrically insulating sheets were placed between the conductive cylinders and the load surfaces in order to ensure that the electrical signal went through the sample. The resistance of the carbon fillers was measured using an Agilent 34401A multimeter (Keysight Technologies, Santa Rosa, CA, USA).

The complex permittivity of the samples was measured in the GHz range by means of a cylindrical coaxial cell (EpsiMu toolkit [33]), containing the sample as a dielectric spacer between inner and outer conductors, whose diameters are 0.3 cm and 0.7 cm, respectively, according to the methodology reported by Torsello et al. [25]. Two conical parts link the cell to standard connectors, allowing to keep the characteristic impedance to 50 Ω, thus avoiding mismatch and energy loss. The cell is connected to a Rohde

Schwarz ZVK Vector Network Analyzer, suitably calibrated, and measurements are analyzed with a two-port transmission line technique. The electromagnetic properties of the sample are determined by de-embedding, using Nicolson–Ross–Weir transmission/reflection algorithm [34].

Results

Characterization of HFB

The typical morphology of pyrolyzed hemp fibers is shown in Fig. 1.

HFB is characterized by the presence of millimetric fibers (Fig. 1 a) with an average size of up round 50 μm. The single fiber retains the original structure as also reported by Kabir et al. [35]. As shown in Fig. 1 b, HFB displays an external part that was originally composed by a mix of cellulose, lignin and hemicellulose wrapped around to a more compact inner section originally consisting of cellulose. During the pyrolytic treatment, the temperature gradient and the differential release of volatile organic matter from the core of the fiber induce a partial detachment of the external part of the fiber and the appearance of some cracks on the inner part. No channels in the single fibers are observable, probably as a consequence of their collapse during the thermal degradation [36].

Besides, the pyrolytic conversion of hemp fibers induces a chemical modification of the structure of pristine fibers as easily shown in the FTIR and Raman spectra (Fig. 2).

As shown in Fig. 2 a, the typical FTIR spectrum of neat hemp fibers displays a very intense and broad υ_{OH} band, due to the massive presence of cellulose as confirmed also by the δ_{CO} at around 1029 cm^{-1}. Besides, an intense $\upsilon_{C=C}$ at 1656 cm^{-1} ascribed to the presence of lignin aromatic moieties is visible. Conversely, the FTIR spectrum of HFB displays only two appreciable weak bands attributable to $\upsilon_{C=C}$ at 1647 cm^{-1} and $\upsilon_{C\text{-}O}$ at 1392 cm^{-1}. The disappearance of functionalities in HFB is a consequence of pyrolytic degradation that promotes the formation of sp^2 carbon structures [37] as clearly shown by the Raman spectrum of Fig. 2 b. The Raman spectrum of HFB displays very intense and not well resolved D and G peak with an appreciable amount of intercomponents, suggesting the presence of a materials that was graphitic but highly disordered [38]. This finding is supported by the high value of I_D/I_G ratio (equal to 1.24) and by a 2D region not well resolved.

The HFB electrical properties that are found to be dependent the degree of carbonization [39] are evaluated according with the methodology reported by Noori et al. [40]; the obtained data are shown in Fig. 3.

As shown in Fig. 3a, the HFB conductivity increases as a function of temperature T, but not exponentially. Two different power-law scalings ($\sigma \propto T^{\beta}$) are observed at low T ($T \lesssim 20K, \beta = 0.16$) and high T ($T \gtrsim 100K, \beta = 0.22$), with a crossover at intermediate T. Similar behaviors have been reported in biochar derived by pyrolysis of tea leaves [40] and in superhard carbon nanocomposites[40]. According to the theory of the insulator-to-metal transition (IMT) [41–43], power-law dependences of the conductivity with temperature are typical of the quantum critical regime of the IMT, with $\beta < 1/3$ and $\beta > 1/3$ being associated with its metallic and insulating sides. The values of β observed in HFB therefore place it firmly in the metallic side of the IMT, albeit closer to the

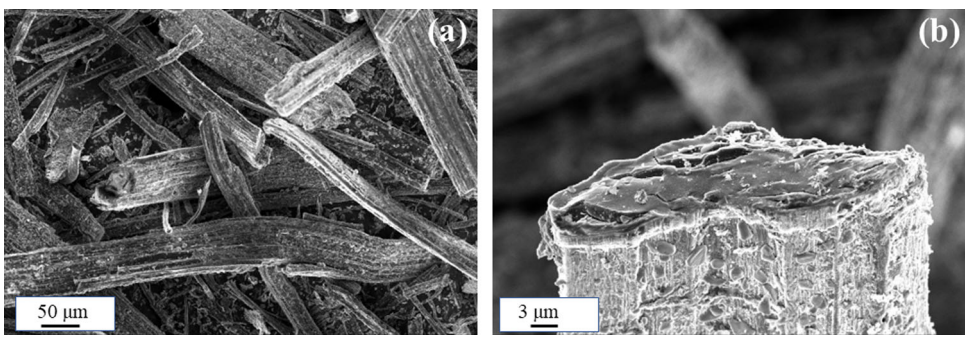

Figure 1 FESEM micrographs of a bundle of pyrolyzed hemp fibers (**a**) and of a single fiber (**b**).

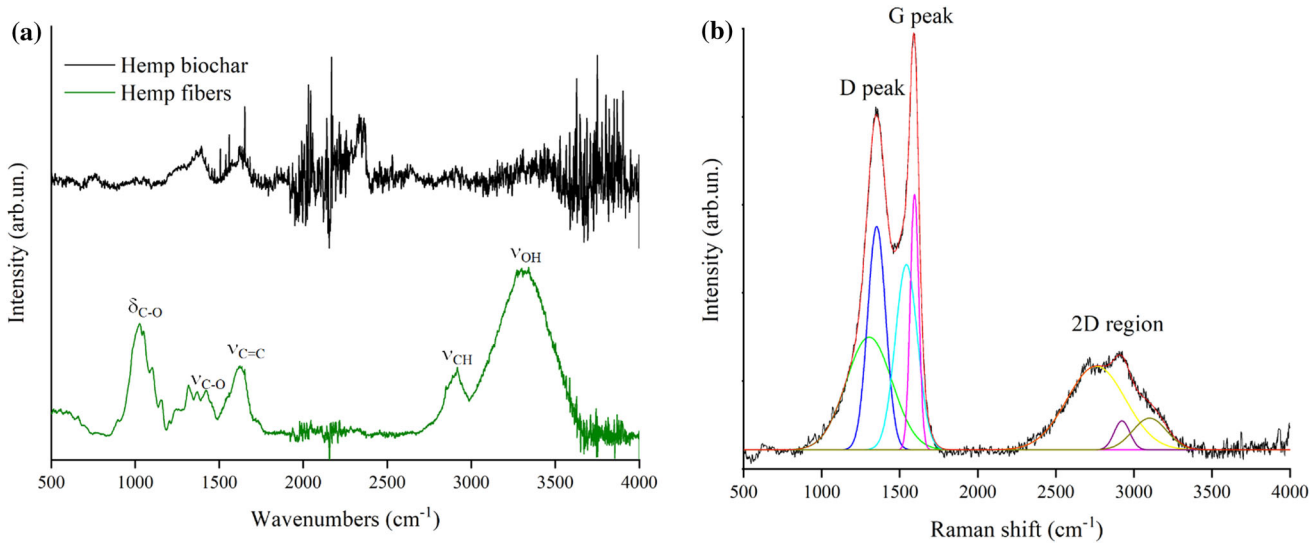

Figure 2 (**a**) FTIR spectra (ATR mode) of pristine (green) and pyrolyzed (black) hemp fibers and (**b**) Raman spectra HFB in the range from 500 to 4000 cm^{-1}.

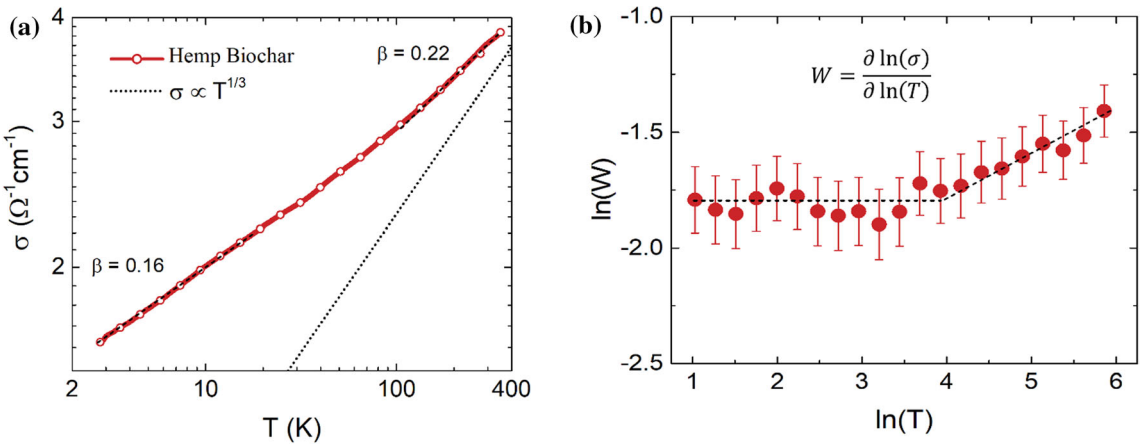

Figure 3 DC electrical conductivity (**a**) and reduced activation energy (**b**) measured as a function of temperature in single carbonized hemp fibers.

transition with respect to tea-derived biochar ($\beta = 0.07$) [40]. This quantum critical behavior is further confirmed through Zabrodskii analysis [44] of the reduced activation energy $W = \frac{\partial \ln \sigma}{\partial \ln T}$. As shown in Fig. 3b, W is constant at low T and it mildly increases at higher T, whereas W would decrease with increasing T in hopping-type transport—as so far observed in biochars derived from the pyrolysis of cotton fibers only [23]. In agreement with Pukha et al. [45], we therefore exclude charge-carrier hopping as a significant source of conductivity in HFB and ascribe its dominant DC electric transport mechanism to direct tunneling between graphite nanocrystals across sp^3 boundaries.

Characterization of epoxy/hemp fiber biochar composites

Optical microscopy was used for investigating the distribution of HFB in the epoxy matrix; the typical images are shown in Fig. 4.

As shown in Fig. 4 a, pyrolyzed fibers (white circled) preserve their sub-millimetric length and are well embedded into the polymeric matrix. The single fiber (Fig. 4 c) does not show any appreciable modification in size compared with what observed before its dispersion within the epoxy resin. At higher HFB loadings, the probability to find fibre bundles increases, as shown in Fig. 4b for EP/HFB 90/10.

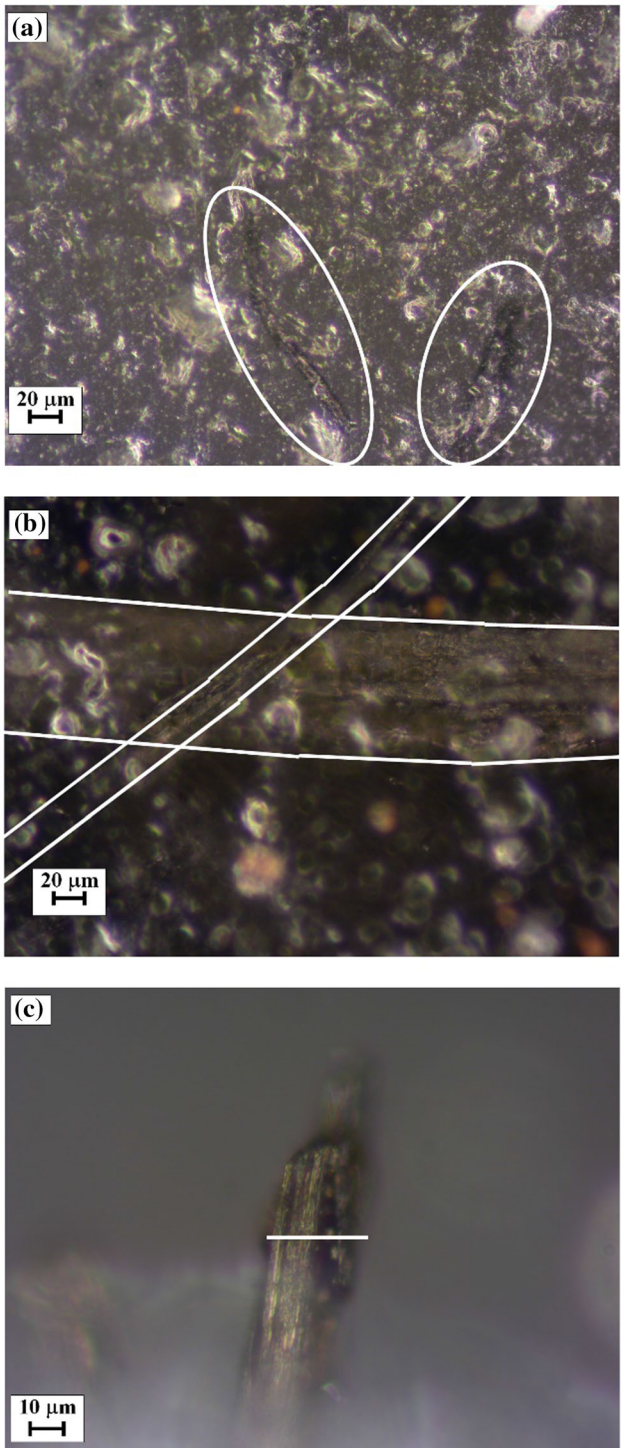

Figure 4 Optical microscopy captures of epoxy composites filled with 1 wt% (**a**) and 10 wt% (**b**) of HFB; a snapshot on a single embedded carbonized hemp fiber (**c**).

Thermal behavior in both nitrogen and air atmosphere is reported in Fig. 5; T_{10}, T_{max} and the residue at 800 °C are summarized in Table 1. A one-stage degradation process and a two-stage degradation process are observed for all the tested samples in N_2 and air atmosphere, respectively.

In nitrogen, the addition of HFB in the epoxy matrix induces a remarkable decrease in the T_{max} at high HFB loadings: this phenomenon is probably due to the radical degradation of epoxy matrix promoted by the surface of HFB. In fact, the hydroxyl, carbonyl and carboxylic groups on the filler surface may induce the break of the nitrogen-carbon bond at high temperature [46]. However, this decrease is not correlated with the HFB loading. T_{10} remains almost constant.

In air, T_{10} and T_{max1} are slightly higher with respect to the unfilled polymer network. Again, these variations are not directly related to the HFB loading. However, T_{max2} seems more clearly affected by presence of the filler and decreases by increasing the HFB amount.

The DSC thermograms of the unfilled epoxy network and its composites are shown in Fig. 6. Exothermic peaks above T_g are not visible in the curves, implying that the adopted experimental conditions are sufficient to promote the creation of a fully cured network. EP has a T_g of 116 °C, which lowers to 96 °C by adding 2.5 wt% of HFB. The well-distributed fibers in this composite were able to penetrate the epoxy resin inter-chain gap, limiting the production of crosslinks and therefore lowering the T_g. As the amount of HFB in the system grows, more fiber bundles develop as observed by optical microscopy. As a result, the chances of these agglomerates penetrating the resin inter-chain spacing are reduced, minimizing the crosslinking restriction effect. Thus, by increasing the HFB content (i.e., at 5 and 7.5 wt%), the T_g rises and approaches that of unfilled polymer at 10 wt% of HFB loading.

To get useful insights into the viscoelastic behavior of the epoxy composite materials, dynamic mechanical analyses were carried out from room temperature to 160 °C.

Figure 7a shows the effect of temperature and filler loading on storage modulus values. In the glassy state, in comparison with unfilled epoxy resin, the composites show an increase in storage modulus values, suggesting a reinforcing effect exerted by HFB. At higher filler loadings, the composite storage modulus improves even more. In particular, the storage modulus for neat epoxy at 40 °C is about 1400 MPa, whereas for 10% of filler loading, the

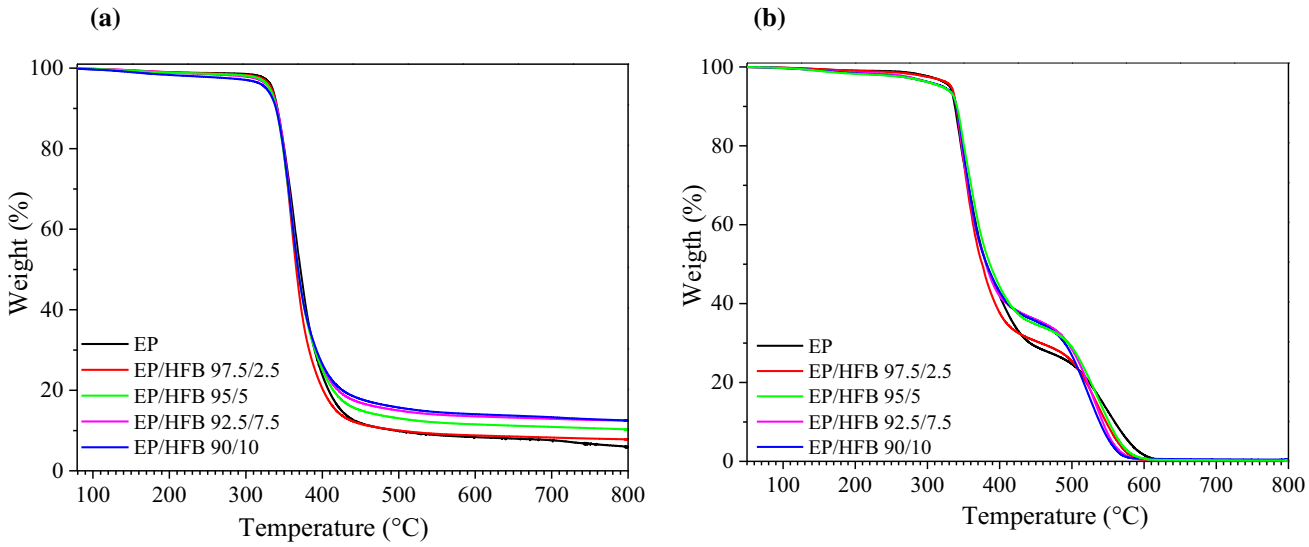

Figure 5 TGA analysis of epoxy/HFB composites run in **a** nitrogen and **b** in air.

Table 1 Thermogravimetric data of the epoxy system and its composites with HFB, in nitrogen and in air atmosphere

	N_2			Air			
	T_{10} (°C)	T_{max} (°C)	Residue (%) @800 °C	T_{10} (°C)	T_{max1} (°C)	T_{max2} (°C)	Residue (%) @800 °C
EP	341	367	5.8	337	343	551	–
EP/HFB 97.5/ 2.5	341	359	8.9	340	348	539	–
EP/HFB 95/5	342	360	10.3	341	347	537	–
EP/HFB 92.5/7.5	341	360	12.2	340	349	531	–
EP/HFB 90/10	339	360	12.5	340	349	524	–

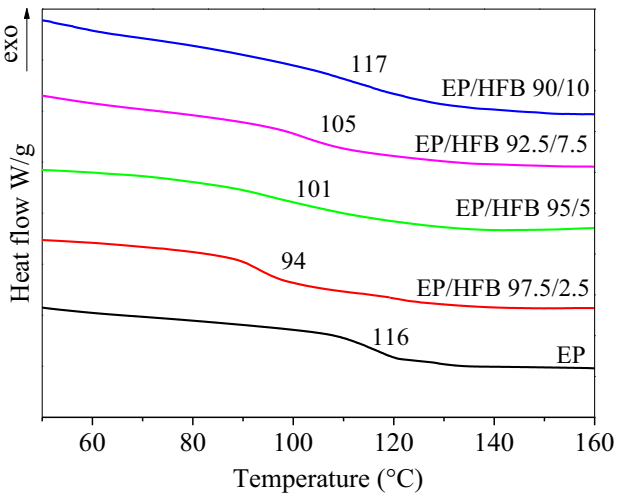

Figure 6 DSC traces of epoxy-hemp fiber biochar composites.

storage modulus value is around 2310 MPa. The creation of a filler matrix network, which acts as an energy barrier for chain mobility, results in easy load transfer and in increased modulus. In the rubbery state (e.g., at 140 °C), the composites show slightly higher storage modulus values than the unfilled epoxy resin. This finding can be ascribed to the higher viscosity of the epoxy matrix as a result of the inclusion of HFB slowing down the deformation rate. The increase in storage modulus value with the rise in filler loading has also been found for other epoxy composites reinforced with wood fibers and more in general in other fiber-loaded composites. [47–49]

Figure 7b displays the loss tangent (tanδ) as a function of the temperature for all the systems investigated. The glass transition in the dynamic mechanical test is measured as the maximum of the tanδ peak, which is associated with the movement of small groups and macromolecular segments within the initially frozen structure of the epoxy resin. Therefore, the higher the tanδ peak value, the greater

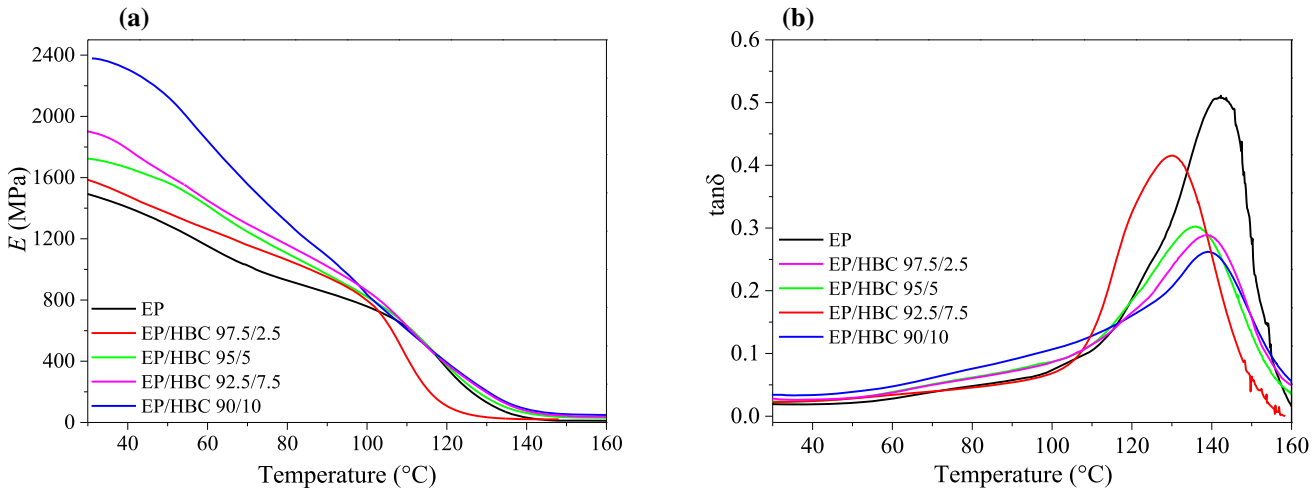

Figure 7 **a** Storage modulus and **b** tanδ of EP and EP-HFB composites.

is the molecular mobility [48] and hence the higher are the damping characteristics.

The T_g value for pure epoxy samples is 142 °C, whereas it ranges from 130 to 140 °C for the composites, hence further supporting the behavior already described for DSC analyses; however, the T_g values determined with dynamic-mechanical analyses are higher with respect to the corresponding DSC values: This difference is ascribed to frequency effect as clearly reported in the literature [50].

Furthermore, at the glass transition temperature, pristine epoxy sample shows the highest damping factor value. Due to the constrained molecular movement in the polymer chain in the presence of pyrolyzed hemp fibers, this value decreases as the filler loading increases, minimizing energy dissipation. Another further possible explanation refers to the decrease in volume of the epoxy matrix able to dissipate the vibration energy [47].

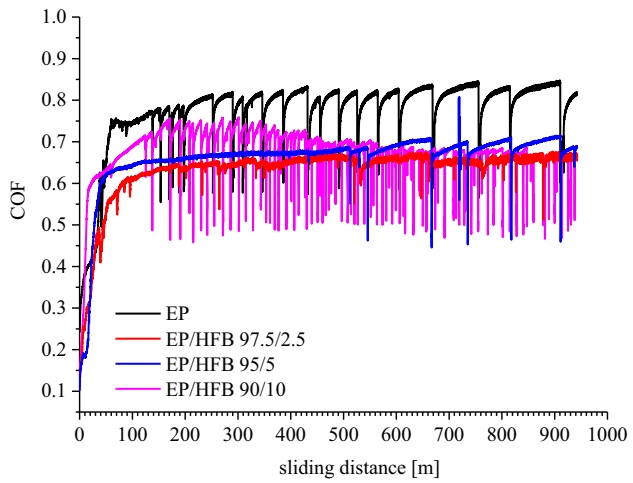

Figure 8 Coefficient of friction (COF) as a function of sliding distance for the epoxy resin and its composites.

Figure 8 depicts the COF as a function of the sliding distance for epoxy resin and some composites representative of low, medium and high biochar loadings. The roughness, steady COF, wear depth and wear rate, together with the hardness (shore D) of the systems, are summarized in Table 2. The peculiar fluctuation of the friction coefficient of the polymer composites indicates the occurrence of a stick–slip phenomenon due to the plowing motion of the harder steel ball on the softer substrate [51].

Table 2 highlights a reduction of the composite COF with respect to the unfilled resin. More in detail, the composites display a COF 20% lower with respect to that of unfilled epoxy resin. The amount of HFB does not significantly influence the COF values. The decrease in friction observed for the epoxy composites is also accompanied by a significant reduction of the wear rate (Table 2) with respect to the unfilled resin. This finding can be due to the increased hardness (Table 2) and rigidity of the composites that increase the resistance of composite material to wear. The collected data show a Spearman coefficient of up to 0.7 proving a light positive correlation between HFB loafing and shore D hardness [52].

SEM micrographs of worn surfaces (of both epoxy systems and 100Cr6 counterbodies, Fig. 9) confirm the observations previously discussed. However, they also give important information for the comprehension of the wear mechanism involved in the pair epoxy resin steel. Unfilled epoxy (Fig. 9A) shows

Table 2 Roughness, coefficients of friction, wear depth and steady-state wear rates for epoxy resin its composites

	R_a (μm)*	COF	Depth (μm)	Wear rate ($\times 10^{-5}$ $mm^3/N{\cdot}m$)	Shore D**
EP	0.78 ± 0.11[a]	0.82	30.6 ± 3.5	7.52	88.4 ± 0.6[a]
EP/HFB 97.5/2.5	0.79 ± 0.10[a]	0.65	9.9 ± 1.4	1.54	90.5 ± 0.4[b]
EP/HFB 95/5	0.71 ± 0.13[a]	0.67	11.9 ± 1.6	1.75	91.8 ± 0.6[c]
EP/HFB 90/10	0.78 ± 0.15[a]	0.67	19.3 ± 1.9	3.88	91.7 ± 0.6[c]

*Values are given as mean ± standard deviation. Different letters in the same column for R_a (μm) indicate significantly differences ($p < 0.05$) when analyzed by Duncan's multiple range test

**Values are given as mean ± uncertainty. Different letters in the same column for shore D indicate significantly differences ($p < 0.05$) when analyzed by Duncan's multiple range test

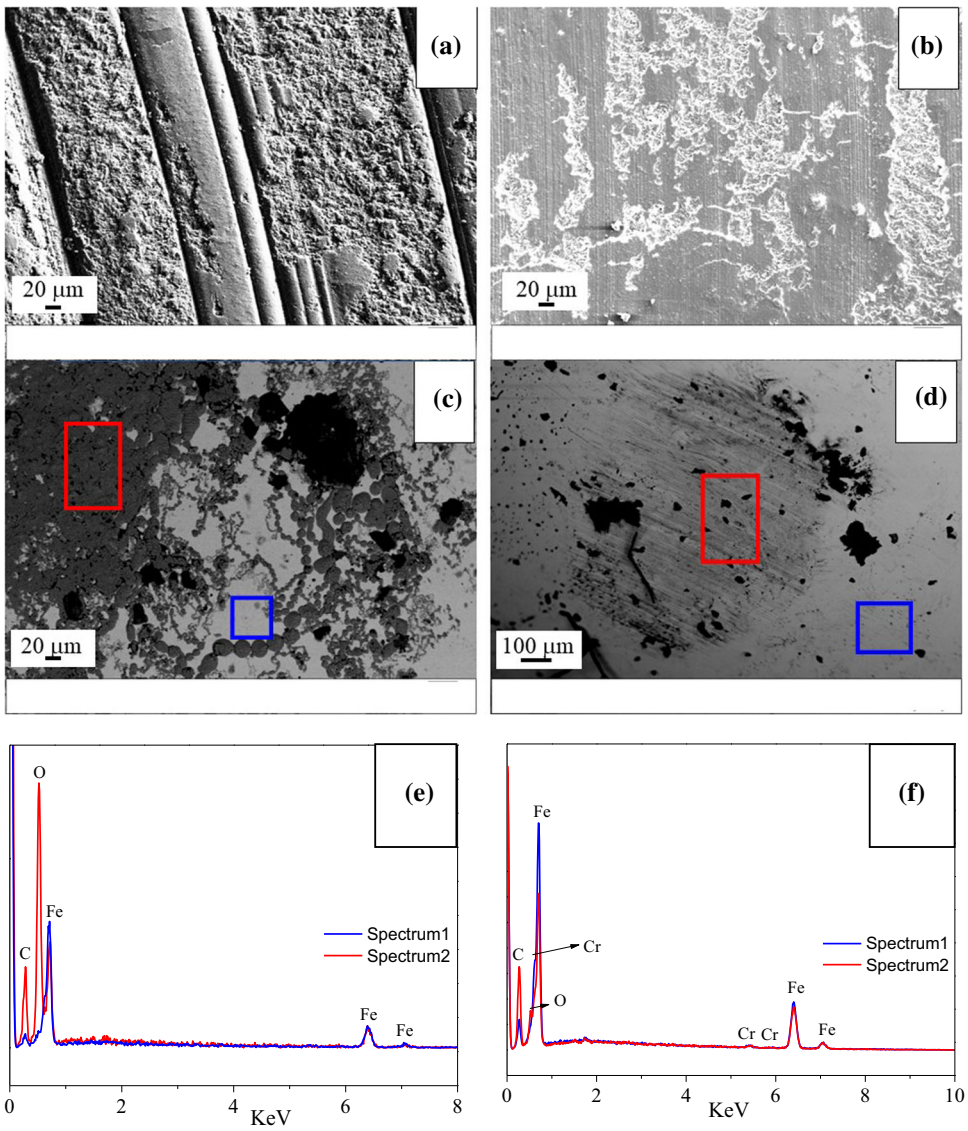

Figure 9 SEM micrographs of **a** epoxy resin and **b** EP/HFB 90/10 composite worn surfaces. SEM micrograph obtained by using backscattered electron of steel ball against **c** unfilled epoxy resin and **d** EP/HFB 90/10 composites. EDX results of steel ball against **e** unfilled epoxy resin and **f** EP/HFB 90/10 composites..

severe wear losses, whereas the worn surface of EP/HFB 90/10 composite (reported as example for the composites in Fig. 9B) is much smoother and the signs of adhesion, deformation and exfoliation of epoxy are significantly reduced. Considering steel ball against unfilled epoxy resin (Fig. 9C), a transfer film appears on the steel surface. Based on the EDX results, outside this film (Fig. 9E—blue spectrum),

the elements are mainly Fe and Cr (only small amounts of C and O are detectable) representative of the ball element. Conversely, main elements of adhesive transfer film (Fig. 9E—red spectrum) include C, O and Fe, indicating both the formation of iron oxides and the presence of polymer debris. As far as the steel ball against epoxy composite (Fig. 9D) is concerned, the worn surface is not covered with the adhesion layer found before. The EDX spectra (Fig. 9F) confirm this result. In fact, by observing the worn steel surface (Fig. 9F—red spectrum), the relative intensity of the O signal with respect to C peak is more compatible with the absence of oxidated species and the presence of polymer composite debris.

The oxidation of steel assisted by a polymer matrix we have found in this work is not completely new in literature [53] and is called chemo-mechanical autocatalytic mechanism of destruction of steel. The macromolecules of the polymer surface crack under the action of severe shear stresses and produce active free radicals and a series of mechano-chemical reactions occur between the two surfaces, resulting in the formation of chemical reaction film on the steel surface. This film is mainly composed by Fe-polymer compound and iron oxides as detected by EDX. Conversely, as far as the composites are concerned, the presence of HFB hinders/reduces the chemical reactions between steel and polymer and the wear mechanism proceeds with the formation of transfer films prevalently made of polymer composite debris as confirmed by EDX.

Thus, the different composition of the adhesion films between the pair epoxy–steel is responsible for higher COF values found in the case of the unfilled epoxy resin with respect to the composites. In the latter, the presence of HFB plays a crucial role in reducing the amount of oxidated species in the tribofilm. Several reasons that may justify this finding can be mentioned: first, HFB, by increasing the rigidity and hardness of the composites, could reduce the amount of polymer debris. This, in turn, reduces the amount of material that can react with the steel. Besides, based on the structural properties (see Raman discussion), it could be hypothesized a higher thermal conductivity for HFB with respect to epoxy resin. Thus, HFB could dissipate better the friction heat by reducing the temperature at the polymer–steel interface and hindering the chemical reactions.

From a general point of view, the combination of epoxy resin with HFB is an efficient method to improve the wear resistance of epoxy resin. Compared with unfilled epoxy, the composites show a lower friction coefficient and wear rate. In addition, the chemo-mechanical autocatalytic mechanism of destruction of steel seems reduced by the presence of HFB.

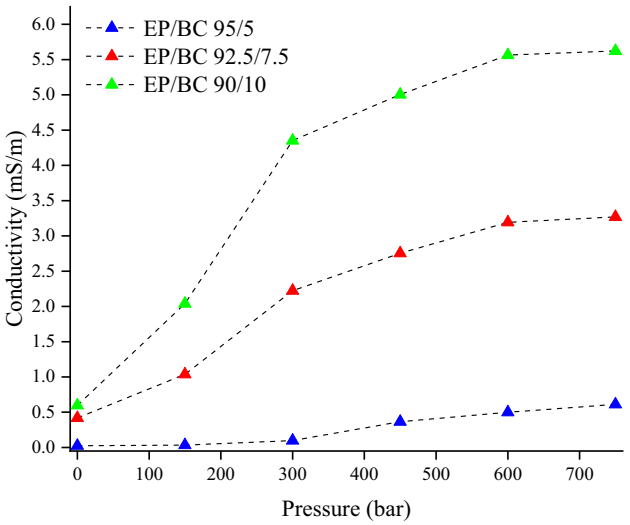

Figure 10 Conductivity of HFB-containing epoxy composites in the pressure range from 1 and 750 bar.

The electrical conductivity was first investigated by applying a pressure ranging from 1 up to 750 bar (Fig. 10).

The composites containing HFB loadings below 5 wt% do not show any appreciable conductivity as the unfilled epoxy matrix. All the other composites show a negligible conductivity at 1 bar ranging from 0.02 mS/m (EP/BC 95/5) up to 0.6 mS/m (EP/BC 90/10). According to the filler loadings, EP/BC 90/10 sample shows the highest conductivity, reaching 6 mS/m at 750 bar.

The observed conductivity values are comparable with those reported for loading exceeding 15 wt% of coffee-derived biochar dispersed into an epoxy matrix [24], but considerably lower compared to cotton-derived biochar fibers produced at 1000 °C and dispersed into poly(vinyl alcohol) [23]. The improvement upon coffee-derived biochar is reasonably due to the aspect ratio of the HFB that allowed to reach percolation threshold in a more effective way. Conversely, the lower performance of HFB compared with cotton-derived biochar fibers is reasonably due to the improved aspect ratio of pure cellulosic materials as compared with lignocellulosic hemp fibers. Nevertheless, HFB composites show a

Table 3 Comparison of electrical conductivity of different carbonaceous filler-based epoxy composites

Filler	Loading	Conductvity (S/m)	Reference
Coffee biochar @ 1000 °C[a]	15 wt%	2.02	[24]
Carbonized cellulose nanocrystals @1000 °C[a]	10 wt%	3.01	[54]
MWCNTS	0.4 wt%	0.02	[55]
MWCNTS/carbon fibres	56 vol.%	> 20	[56]
Carbon fibres (unidirectional prepreg)	61 vol.%	10	[57]
Graphene	0.4 vol.%	0.001	[58]
Carbon black[a]	15 wt%	0.02	[24]
HFB produced at 1000 °C	10 wt%	6	Present work

[a]Under pressure measurement

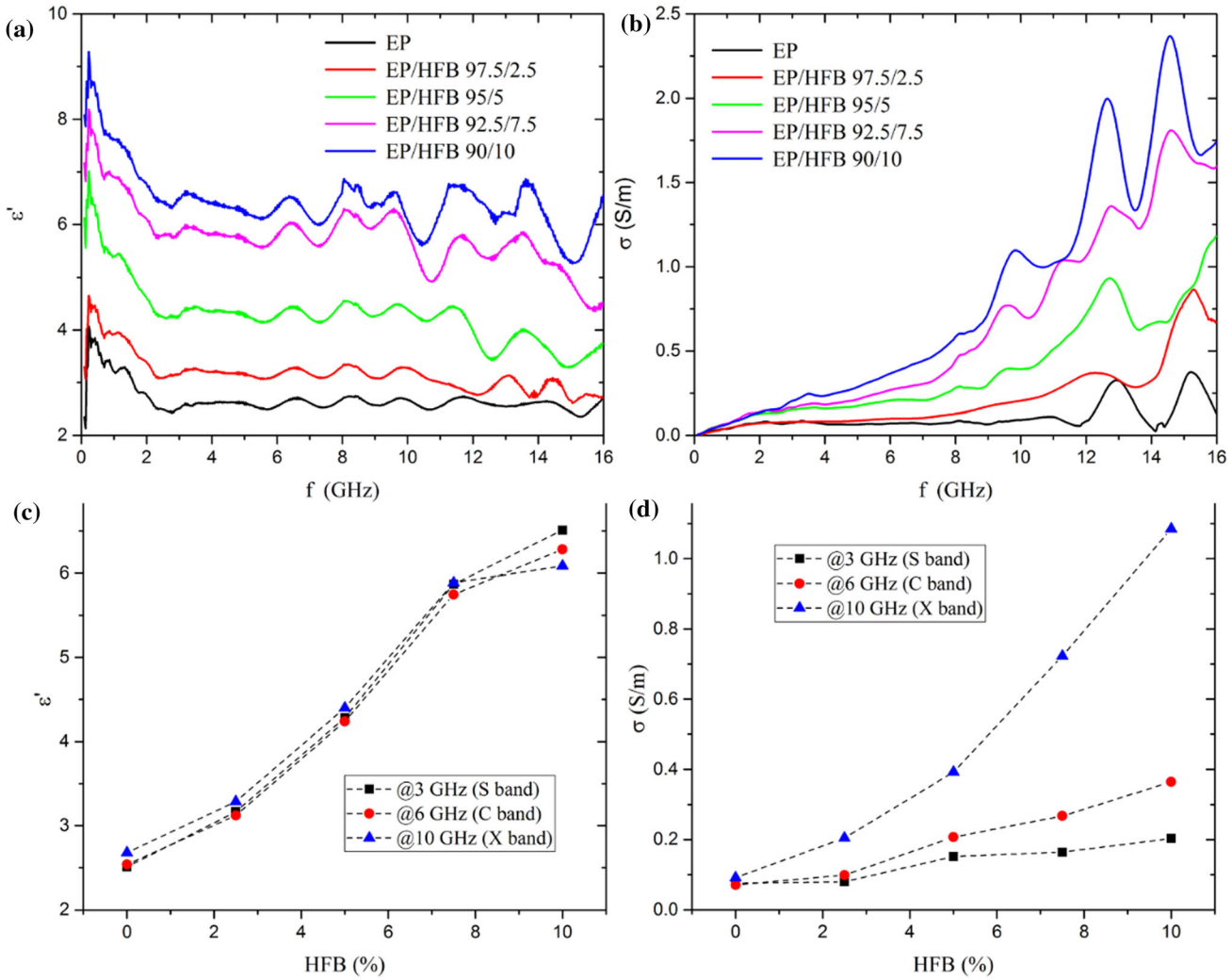

Figure 11 Real part of the complex permittivity **a** and conductivity **b** as a function of frequency, and complex permittivity **c** and conductivity **d** as a function of HFB weight fraction at representative frequencies for communication microwave bands.

remarkably high conductivity for low filler loadings compared with other carbonaceous fillers as reported in Table 3.

The high-frequency electrical response of the composite can be fully characterized by the real part of the complex permittivity (ε') and the conductivity (σ). These two parameters are reported in Fig. 11 as a

function of frequency in the 100 MHz–16 GHz range and of HFB loading in the epoxy composites.

The real permittivity curves show a slight initial decrease when frequency increases, followed by a plateau, whereas conductivity increases monotonically with frequency, as expected. For the composites, the trends of both ε' and σ increase are quite linear with the biochar loading, and their strong variations for a modest HFB content allow a fine-tuning of the composite material properties, which is promising for such applications as microwave shielding [59].

Conclusions

The utilization of waste hemp fiber to produce fibrous biochar has not been investigated yet in depth. In this work, we reported the use of hemp-derived carbon fibers obtained by pyrolysis at 1000 °C for the production of conductive composites with enhanced mechanical and tribological properties.

The storage modulus of the composites increases with the increase in HFB due to the creation of a filler matrix network, which acts as an energy barrier for chain mobility, resulting in easy load transfer and in increased modulus. The use of HBF is also an efficient method to improve the wear resistance of epoxy resin. In fact, compared with unfilled epoxy, the composites show lower friction coefficient and wear rate values. Also, the presence of HFB induces a remarkable increase in electrical conductivity that approaches 6 mS/m in the presence of 10 wt% of HBF. A similar trend is also observed for the high-frequency measurements.

The new approach in using waste hemp fibers, proposed in this work, may favor an increased use of this waste biomass for several key application sectors, including automotive and aeronautical industry. Moreover, the advantage in using waste carbon fiber as compared to the petroleum-based carbon filler for composites fabrication is its waste utilization and reuse resources which aids the circular economy, sustainability and reduction of environmental footprint.

Acknowledgements

The authors acknowledge the support from the Regione Campania in the framework of the project titled “Canapa Campana in Fibra (CCF)”—PSR Campania 2014/2020.

Declarations

Conflict of interest The authors declare that they have no conflict of interest.

Ethical approval This research does not include experiments involving human tissue and does not contain any studies with human participants or animals performed by any of the authors.

References

[1] Liu S, Chevali VS, Xu Z, Hui D, Wang H (2018) A review of extending performance of epoxy resins using carbon nanomaterials. Compos B Eng 136:197–214

[2] Carter J, Emmerson G, Faro CL, McGrail P, Moore D (2003) The development of a low temperature cure modified epoxy resin system for aerospace composites. Compos A Appl Sci Manuf 34(1):83–91

[3] Mazzon E, Habas-Ulloa A, Habas J-P (2015) Lightweight rigid foams from highly reactive epoxy resins derived from vegetable oil for automotive applications. Eur Polymer J 68:546–557

[4] Zaman I, Phan TT, Kuan H-C, Meng Q, La LTB, Luong L, Youssf O, Ma J (2011) Epoxy/graphene platelets

nanocomposites with two levels of interface strength. Polymer 52(7):1603–1611

[5] Zakaria MY, Sulong AB, Sahari J, Suherman H (2015) Effect of the addition of milled carbon fiber as a secondary filler on the electrical conductivity of graphite/epoxy composites for electrical conductive material. Compos B Eng 83:75–80

[6] Katiyar JK, Sinha SK, Kumar A (2016) Effects of carbon fillers on the tribological and mechanical properties of an epoxy-based polymer (SU-8). Tribol-Mater Surfaces Interfaces 10(1):33–44

[7] Kumar A, Bhattacharya T, Hasnain SM, Nayak AK, Hasnain S (2020) Applications of biomass-derived materials for energy production, conversion, and storage. Mater Sci Energy Technol

[8] Pal L, Lucia LA (2019) Renaissance of industrial hemp: a miracle crop for a multitude of products. BioResources 14(2):2460–2464

[9] Crini G, Lichtfouse E, Chanet G, Morin-Crini N (2020) Applications of hemp in textiles, paper industry, insulation and building materials, horticulture, animal nutrition, food and beverages, nutraceuticals, cosmetics and hygiene, medicine, agrochemistry, energy production and environment: a review. Environ Chem Lett 18:1451–1476

[10] Ruano G, Bellomo F, Lopez G, Bertuzzi A, Nallim L, Oller S (2020) Mechanical behaviour of cementitious composites reinforced with bagasse and hemp fibers. Constr Build Mater 240:117856

[11] Scarponi C, Messano M (2015) Comparative evaluation between E-Glass and hemp fiber composites application in rotorcraft interiors. Compos B Eng 69:542–549. https://doi.org/10.1016/j.compositesb.2014.09.010

[12] Mishra S, Naik J (1998) Absorption of water at ambient temperature and steam in wood–polymer composites prepared from agrowaste and polystyrene. J Appl Polym Sci 68(4):681–686

[13] Rouison D, Couturier M, Sain M, MacMillan B, Balcom B (2005) Water absorption of hemp fiber/unsaturated polyester composites. Polym Compos 26(4):509–525

[14] Bambach MR (2020) Direct Comparison of the Structural Compression Characteristics of Natural and Synthetic Fiber-Epoxy Composites: Flax, Jute, Hemp. Glass Carbon Fibers Fibers 8(10):62

[15] Li M, Ali Z, Wei X, Li L, Song G, Hou X, Do H, Greer JC, Pan Z, Lin C-T (2021) Stress induced carbon fiber orientation for enhanced thermal conductivity of epoxy composites. Compos B Eng 208:108599

[16] Kosiński P, Brzyski P, Szewczyk A, Motacki W (2018) Thermal properties of raw hemp fiber as a loose-fill insulation material. J Nat Fibers 15(5):717–730

[17] Kymäläinen H-R, Sjöberg A-M (2008) Flax and hemp fibres as raw materials for thermal insulations. Build Environ 43(7):1261–1269

[18] Naik J, Mishra S (2005) Studies on electrical properties of natural fiber: HDPE composites. Polym-Plast Technol Eng 44(4):687–693

[19] Branca C, Di Blasi C, Galgano A (2017) Experimental analysis about the exploitation of industrial hemp (Cannabis sativa) in pyrolysis. Fuel Process Technol 162:20–29

[20] Nan N, DeVallance DB (2017) Development of poly(vinyl alcohol)/wood-derived biochar composites for use in pressure sensor applications. J Mater Sci 52(13):8247–8257. https://doi.org/10.1007/s10853-017-1040-7

[21] Ma Y, Li Y, Zeng Y-P (2021) The effects of vacuum pyrolysis conditions on wood biochar monoliths for electrochemical capacitor electrodes. J Mater Sci 56(14):8588–8599

[22] Giorcelli M, Bartoli M, Sanginario A, Padovano E, Rosso C, Rovere M, Tagliaferro A (2021) High-temperature annealed biochar as a conductive filler for the production of piezoresistive materials for energy conversion application. ACS Appl Electron Mater 3(2):838–844. https://doi.org/10.1021/acsaelm.0c00971

[23] Bartoli M, Torsello D, Piatti E, Giorcelli M, Sparavigna AC, Rovere M, Ghigo G, Tagliaferro A (2022) Pressure-responsive conductive poly(vinyl alcohol) composites containing waste cotton fibers biochar. Micromachines 13(1):125

[24] Giorcelli M, Bartoli M (2019) Development of coffee biochar filler for the production of electrical conductive reinforced plastic. Polymers 11(12):17

[25] Torsello D, Ghigo G, Giorcelli M, Bartoli M, Rovere M, Tagliaferro A (2021) Tuning the microwave electromagnetic properties of biochar-based composites by annealing. Carbon Trends 100062. https://doi.org/10.1016/j.cartre.2021.100062

[26] Khan A, Savi P, Quaranta S, Rovere M, Giorcelli M, Tagliaferro A, Rosso C, Jia CQ (2017) Low-cost carbon fillers to improve mechanical properties and conductivity of epoxy composites. Polymers 9(12):642

[27] Chang BP, Rodriguez-Uribe A, Mohanty AK, Misra M (2021) A comprehensive review of renewable and sustainable biosourced carbon through pyrolysis in biocomposites uses: Current development and future opportunity. Renew Sustain Energy Rev 152:111666

[28] Cui L-J, Geng H-Z, Wang W-Y, Chen L-T, Gao J (2013) Functionalization of multi-wall carbon nanotubes to reduce the coefficient of the friction and improve the wear resistance of multi-wall carbon nanotube/epoxy composites. Carbon 54:277–282

[29] Renato D, Felice G (2010) Macchina sfibratrice per canapa ad uso industriale
[30] Yee R, Stephens T (1996) A TGA technique for determining graphite fiber content in epoxy composites. Thermochim Acta 272:191–199
[31] Myers L, Sirois MJ (2004) Spearman correlation coefficients, differences between. Encycl Stat Sci 12:1
[32] Österle W, Deutsch C, Gradt T, Orts-Gil G, Schneider T, Dmitriev A (2014) Tribological screening tests for the selection of raw materials for automotive brake pad formulations. Tribol Int 73:148–155
[33] Ba D, Sabouroux P (2010) Epsimu, a toolkit for permittivity and permeability measurement in microwave domain at real time of all materials: Applications to solid and semisolid materials. Microw Opt Technol Lett 52(12):2643–2648
[34] Baker-Jarvis J, Vanzura EJ, Kissick WA (1990) Improved technique for determining complex permittivity with the transmission/reflection method. IEEE Trans Microw Theory Tech 38(8):1096–1103
[35] Kabir MM, Wang H, Lau KT, Cardona F (2013) Effects of chemical treatments on hemp fibre structure. Appl Surf Sci 276:13–23. https://doi.org/10.1016/j.apsusc.2013.02.086
[36] Jagdale P, Koumoulos EP, Cannavaro I, Khan A, Castellino M, Dragatogiannis DA, Tagliaferro A, Charitidis CA (2017) Towards green carbon fibre manufacturing from waste cotton: a microstructural and physical property investigation. Manuf Rev 4:10
[37] Chen Y, Syed-Hassan SSA, Xiong Z, Li Q, Hu X, Xu J, Ren Q, Deng Z, Wang X, Su S (2021) Temporal and spatial evolution of biochar chemical structure during biomass pellet pyrolysis from the insights of micro-Raman spectroscopy. Fuel Process Technol 218:106839
[38] Tagliaferro A, Rovere M, Padovano E, Bartoli M, Giorcelli M (2020) Introducing the novel mixed gaussian-lorentzian lineshape in the analysis of the raman signal of biochar. Nanomaterials 10(9):1748
[39] Gabhi RS, Kirk DW, Jia CQ (2017) Preliminary investigation of electrical conductivity of monolithic biochar. Carbon 116:435–442
[40] Noori A, Bartoli M, Frache A, Piatti E, Giorcelli M, Tagliaferro A (2020) Development of Pressure-Responsive PolyPropylene and Biochar-Based Materials. Micromachines 11(4):339
[41] Heeger AJ (2002) The critical regime of the metal-insulator transition in conducting polymers: experimental studies. Phys Scr 2002(T102):30
[42] Piatti E, Galanti F, Pippione G, Pasquarelli A, Gonnelli RS (2019) Towards the insulator-to-metal transition at the surface of ion-gated nanocrystalline diamond films. Eur Phys J Spec Top 228(3):689–696. https://doi.org/10.1140/epjst/e2019-800188-9
[43] Piatti E, Romanin D, Daghero D, Gonnelli RS (2019) Two-dimensional hole transport in ion-gated diamond surfaces: a brief review. Low Temp Phys 45(11):1143–1155
[44] Zabrodskii A, Zinov'eva K, (1984) Low-temperature conductivity and metal-insulator transition in compensate n-Ge. Zh Eksp Teor Fiz 86(2):727–742
[45] Pukha V, Karbovskii V, Rudchenko S, Drozdov A, Maleyev M, Starikov V, Pugachov A (2014) Electronic and optical properties of superhard nanocomposite films obtained from C60 ion beam. Mater Res Express 1(3):035049
[46] Zhou G, Mikinka E, Golding J, Bao X, Sun W, Ashby A (2020) Investigation of thermal degradation and decomposition of both pristine and damaged carbon/epoxy samples with thermal history. Compos B Eng 201:108382. https://doi.org/10.1016/j.compositesb.2020.108382
[47] Jawaid M, Khalil HA, Hassan A, Dungani R, Hadiyane A (2013) Effect of jute fibre loading on tensile and dynamic mechanical properties of oil palm epoxy composites. Compos B Eng 45(1):619–624
[48] Rathore DK, Prusty RK, Kumar DS, Ray BC (2016) Mechanical performance of CNT-filled glass fiber/epoxy composite in in-situ elevated temperature environments emphasizing the role of CNT content. Compos A Appl Sci Manuf 84:364–376
[49] Kumar R, Kumar K, Bhowmik S (2018) Mechanical characterization and quantification of tensile, fracture and viscoelastic characteristics of wood filler reinforced epoxy composite. Wood Sci Technol 52(3):677–699
[50] Landel RF, Nielsen LE (1993) Mechanical properties of polymers and composites. CRC Press, New York, U.S.
[51] Menezes PL, Kailas SV (2009) Influence of surface texture and roughness parameters on friction and transfer layer formation during sliding of aluminium pin on steel plate. Wear 267(9–10):1534–1549
[52] Lyerly SB (1952) The average Spearman rank correlation coefficient. Psychometrika 17(4):421–428
[53] Zhang S, Liu H, He R (2004) Mechanisms of wear of steel by natural rubber in water medium. Wear 256(3–4):226–232
[54] Arrigo R, Bartoli M, Torsello D, Ghigo G, Malucelli G (2021) Thermal, dynamic-mechanical and electrical properties of UV-LED curable coatings containing porcupine-like carbon structures. Mater Today Commun 28:102630
[55] Faiella G, Antonucci V, Buschhorn ST, Prado LASA, Schulte K, Giordano M (2012) Tailoring the electrical properties of MWCNT/epoxy composites controlling processing conditions. Compos A Appl Sci Manuf 43(9):1441–1447. https://doi.org/10.1016/j.compositesa.2012.04.002

[56] Du X, Xu F, Liu H-Y, Miao Y, Guo W-G, Mai Y-W (2016) Improving the electrical conductivity and interface properties of carbon fiber/epoxy composites by low temperature flame growth of carbon nanotubes. RSC Adv 6(54):48896–48904. https://doi.org/10.1039/C6RA09839H

[57] Rehbein J, Wierach P, Gries T, Wiedemann M (2017) Improved electrical conductivity of NCF-reinforced CFRP for higher damage resistance to lightning strike. Compos A Appl Sci Manuf 100:352–360. https://doi.org/10.1016/j.compositesa.2017.05.014

[58] Wajid AS, Ahmed HST, Das S, Irin F, Jankowski AF, Green MJ (2013) High-performance pristine graphene/epoxy composites with enhanced mechanical and electrical properties. Macromol Mater Eng 298(3):339–347. https://doi.org/10.1002/mame.201200043

[59] Torsello D, Bartoli M, Giorcelli M, Rovere M, Arrigo R, Malucelli G, Tagliaferro A, Ghigo G (2021) High Frequency Electromagnetic Shielding by Biochar-Based Composites. Nanomaterials 11(9):2383